Original Article



# $^{18}$F-FDG PET/CT and MR imaging features of liver metastases in gastrointestinal stromal tumors: a cross-sectional analysis

**Qinghu Lyu[1#^], Duanyu Lin[1#], Mingdeng Tang[1], Daojia Liu[1], Jieping Zhang[1], Yuntao Wang[2], Vishal G. Shelat[3], Driss Raissi[4], Vikas Ostwal[5], Xingfa Chen[2], Shengxu Li[1]**

[1]Department of Nuclear Medicine, Clinical Oncology School of Fujian Medical University, Fujian Cancer Hospital, Fuzhou, China; [2]Department of Radiology, Clinical Oncology School of Fujian Medical University, Fujian Cancer Hospital, Fuzhou, China; [3]Department of General Surgery, Tan Tock Seng Hospital, Singapore, Singapore; [4]Division of Interventional Radiology, Department of Radiology, University of Kentucky Medical Center, Lexington, KY, USA; [5]Department of Medical Oncology, Tata Memorial Hospital, Homi Bhabha National Institute, Mumbai, Maharashtra, India

*Contributions:* (I) Conception and design: Q Lyu, S Li, D Lin; (II) Administrative support: D Lin; (III) Provision of study materials or patients: Q Lyu, S Li; (IV) Collection and assembly of data: Q Lyu, D Liu, J Zhang, Y Wang, X Chen; (V) Data analysis and interpretation: Q Lyu, S Li; (VI) Manuscript writing: All authors; (VII) Final approval of manuscript: All authors.

[#]These authors contributed equally to this work.

*Correspondence to:* Shengxu Li. Department of Nuclear Medicine, Clinical Oncology School of Fujian Medical University, Fujian Cancer Hospital, No. 420 Fuma Road, Jinan District, Fuzhou 350014, China. Email: lsx2724@163.com.

**Background:** Early detection of gastrointestinal stromal tumor (GIST) liver metastases is crucial for the management and prognosis. In our experience, GIST liver metastases can display hypermetabolism on $^{18}$F-fluorodeoxyglucose positron emission tomography/computed tomography ($^{18}$F-FDG PET/CT) and marked enhancement on magnetic resonance imaging (MRI), which are uncommon in other tumors before treatment. Most literature focus on the imaging evaluation, prognosis after treatment and less is known about imaging features on both imaging methods before treatment. This study analyzes the imaging features of newly diagnosed GIST liver metastases on $^{18}$F-FDG PET/CT and MRI, with goal of improving diagnostic accuracy.

**Methods:** This retrospective study included 55 patients with pathological or radiographical confirmed GIST liver metastases who underwent PET/CT (n=29), MRI (n=22), or both methods (n=4). PET/CT and MRI interpretation including lesion's morphologic features, number, density or signal intensity, hemorrhage, cystic changes or necrosis, maximum standardized uptake value ($SUV_{max}$) of liver metastases and liver background on PET imaging, degree and pattern of enhancement on MRI were obtained by two experienced nuclear medicine physicians and two radiologists respectively. Data are presented as numbers, percentages, means ± standard deviations or median (interquartile range). The correlation between diameter and $SUV_{max}$ of metastases, and primary tumor $SUV_{max}$ and synchronous liver metastases $SUV_{max}$ were analyzed by Spearman's rank test.

**Results:** On PET/CT visual analysis, 38.9%, 23.9%, and 37.2% of lesions showed significant hypermetabolism, slightly higher metabolism, and equal or lower metabolism than liver, respectively. There was a weak correlation between the diameter and $SUV_{max}$ of liver metastases ($r_s$=0.370, P<0.001), and a moderate correlation between $SUV_{max}$ of synchronous liver metastases and the primary tumors ($r_s$=0.492, P<0.001). On contrast-enhanced MRI, 90.8% of lesions showed heterogeneous enhancement in the arterial phase with the variable presentation, and 74.3% had different enhancement patterns between margins and intratumoral parenchyma.

**Conclusions:** Liver lesions in GIST displaying significant, slight hypermetabolism on $^{18}$F-FDG PET/CT, marked or heterogeneous gradual enhancement within the intratumoral parenchyma with ring-like

^ ORCID: 0000-0003-2770-8909.

enhancement on MRI may denote the diagnosis of liver metastasis. However, GIST liver metastases may also display equal or lower metabolism than liver parenchyma on PET, making small lesions more difficult to diagnose.

**Keywords:** Gastrointestinal stromal tumor (GIST); liver metastases; imaging features; positron emission tomography (PET); magnetic resonance imaging (MRI)

Submitted Jan 02, 2020. Accepted for publication Jan 29, 2020.
doi: 10.21037/atm-22-5181
**View this article at:** https://dx.doi.org/10.21037/atm-22-5181

## Introduction

Gastrointestinal stromal tumors (GISTs) are the most frequent mesenchymal neoplasms of the gastrointestinal tract, accounting for 0.1–3% of all gastrointestinal neoplasms (1,2). GISTs mostly occur in the stomach (60–70%) and small intestine (25–35%), and rarely in the esophagus, colon, appendix, anus, peritoneum, mesentery, retroperitoneum, prostate, and gallbladder (3,4). The liver is one of the most frequent locations for GIST metastasis, and hepatic involvement is observed in 15.9% of patients at initial diagnosis (5). The liver is also the most common location of recurrence after primary tumor resection (63%), and it is the only site of recurrence in 44% of patients (6). Furthermore, the recurrence rate after surgical resection of GIST hepatic metastases from GIST was reported to be 70–77% (7,8). The median disease-free period following initial resection of liver metastasis from GIST is 17 months (8). Therefore, close periodic follow-up during the first year after liver metastasectomy is critical. In addition, liver metastasis from GIST can occur more than 10 years later (25, 29, and 32 years after resection of small intestinal, gastric, and duodenal GIST, respectively), suggesting that a life-long clinical follow-up should be recommended (9-11).

Liver metastasis alone is a factor that involves a worse prognosis in GIST patients. For synchronous liver metastasis, its early diagnosis directly affects the determination of clinical treatment, and may require combined multidisciplinary management from the outset. Indeed, one study reported that liver might play a more dominant role than lung and bone in the prognosis of GIST patients with metastasis. Therefore, more attention should be paid to the status of liver in diagnosis and treatment of GIST (12). Consequently, early detection of liver metastasis is crucial for the management and prognosis of GIST patients. Since the associated clinical symptoms are usually inconspicuous or nonspecific, GIST liver metastases are mainly detected by imaging methods. $^{18}$F-fluorodeoxyglucose positron emission tomography/computed tomography ($^{18}$F-FDG PET/CT) is a widely used imaging modality for diagnosis, staging, efficacy assessment, and detection of recurrence of malignant tumors, which integrates metabolic and anatomical information. $^{18}$F-FDG PET/CT has excellent sensitivity in the detection of liver metastases by integrating the anatomical and metabolic activity features of liver tumors, hence providing more accurate information than two scans performed separately (13). Magnetic resonance imaging (MRI) is considered the primary imaging modality of choice in evaluating liver metastasis because of its superior soft-tissue contrast and direct multiplanar acquisition capability, and the lack of exposure to ionizing radiation (14). MRI and $^{18}$F-FDG PET/CT have proven valuable in the assessment of malignant potential, response to treatment after targeted therapy, detecting tumor recurrence, and evaluation of prognosis in GIST (15-20). While there has been much focus on the management, treatment response, and prognosis of GIST liver metastasis (21-23), few studies have examined the imaging features of GIST liver metastases, especially using functional imaging. In our experience, the imaging findings of GIST liver metastases have been quite different from other common tumors such as colorectal carcinoma, breast cancer, and lung cancer. For example, GIST liver metastases can display different metabolic levels on $^{18}$F-FDG PET/CT and marked enhancement on MRI, which are uncommon in other tumors before treatment. Smaller liver metastases sometimes lack specificity in anatomic imaging, whereas in functional imaging the lesions sometimes appear iso- or hypo-metabolism due to liver radiotracer activity, which may lead to misdiagnosis. Therefore, to improve the diagnostic accuracy and reduce the risk of missed diagnosis and misdiagnosis of GIST liver metastases, we herein summarized the imaging features of GIST liver metastases on $^{18}$F-FDG PET/CT and MRI

 

while reviewing their characteristics at the morphological, blood perfusion, and metabolic levels. We present the following article in accordance with the STROBE reporting checklist (available at https://atm.amegroups.com/article/view/10.21037/atm-22-5181/rc).

## Methods

### *General clinical data*

The study was conducted in accordance with the Declaration of Helsinki (as revised in 2013). The study was approved by the Medical Ethics board of Fujian Cancer Hospital (No. K2022-131-01) and informed consent was taken from all individual participants. Cross-sectional design was used in this study. We selected all patients eligible for this study in Fujian Cancer Hospital, then analyzed the characteristics of GIST liver metastases such as morphology, distribution, metabolism and perfusion, and summarized the imaging features of GIST liver metastases. The clinical and imaging data of all GIST patients with suspected liver metastases on PET/CT or MR between January 2011 and December 2021 were retrospectively reviewed. The number of cases in Fujian Cancer Hospital during the study period determined the sample size. GIST patients presenting with liver metastasis were identified. All GISTs were pathologically confirmed by either surgery or biopsy, and all hepatic lesions were confirmed by postoperative pathological or imaging follow-up. The radiographic follow-up period was 6–36 months and lesions were considered metastasis if they satisfied one of the following criteria: (I) the lesion progressed at subsequent follow-up radiographic examinations; (II) the lesion decreased or increased in size or disappeared after molecular targeted therapy; and (III) the lesion presented visible cystic changes after targeted therapy, even if there was no change in size. Cases were excluded if the following situations occurred: (I) patient received targeted therapy within 6 months of when liver metastasis was detected; (II) patient had concurrent other malignancies; and (III) patient had diffuse liver metastases resulting in partial lesions that could not be evaluated.

### *Imaging*

#### PET/CT imaging techniques

PET/CT imaging was performed on a Gemini TF 64 PET/CT instrument (Philips Healthcare, Cleveland, Ohio, USA). The $^{18}$F-FDG was generated from Sumitomo Corporation HM-10 cyclotron, with the radiochemical purity of greater than 95%. Patients fasted for at least 6 hours prior to PET/CT imaging, and blood glucose levels were controlled in the 3.9–7.5 mmol/L range. Following intravenous injection of 185–370 MBq $^{18}$F-FDG, patients then rested quietly for about 60 minutes. All patients were scanned on the machine in the supine position. The acquisition parameters of low-dose CT were 120 kV, 200 mA, matrix 512×512, slice thickness 5 mm. Scanning encompassed from the mid-thigh to the base of the skull. PET images were acquired in 3D mode, with an acquisition time of 1 minute per bed position. CT data were used for the correction of tissue attenuation. PET and CT images, as well as fused PET/CT images, were observed on a Philips EBW workstation.

#### MR imaging techniques

MRI was performed using a 1.5-T MR scanner (20 cases; Signa Excite; GE Healthcare, USA) with an 8-channel phased-array coil and a 3.0 T scanner (6 cases; Achieva, Philips Healthcare, Netherlands) with a 16-channel phased-array coil. A total of 17 patients underwent whole abdominal MRI and 9 patients underwent upper abdominal MRI. Routine MRI sequences included the following: a free-breathing half-Fourier acquisition single-shot turbo spin-echo sequence, a breath-hold T1 weighted dual fast gradient recalled echo sequence (in-phase and opposed-phase), a breath-hold turbo spin-echo T2 weighted fast spin-echo sequence with fat suppression, and free-breathing diffusion-weighted imaging with low and high b-values (b=0, 800 s/mm$^2$, respectively). Dynamic contrast-enhanced MRI was performed using a fat-suppressed T1-weighted three-dimensional gradient echo sequence [time of repetition/time of echo (TR/TE) =4.0–4.5/1.5–2.0 ms, flip angle 15°, matrix 180×320, slice thickness 5.0–6.0 mm, field of view 440×440 mm]. After intravenous injection of 0.1–0.15 mmol/kg contrast material [Gadobenate Dimeglumine (19 cases) or Magnevist (7 cases)] at a rate of 2.5 mL/s, the arterial phase (25 s), portal venous phase (60 s), and the delayed phase (180 s) images were acquired. The hepatobiliary phase images of 6 patients were obtained 1 hour after injection.

### *Image analysis*

For PET/CT imaging analysis, PET, CT, fused PET/CT, and whole-body maximum intensity projection (MIP) images were evaluated by two experienced nuclear

 

medicine physicians using the double-blinded method. Any discrepancies were resolved through discussion to reach a consensus between the two physicians. The location, morphology, size, margin, density, $SUV_{max}$ and the number of liver metastases were recorded in detail. A region of interest (ROI) was placed in the lesion, including the highest radiotracer uptake area, and maximum standardized uptake value ($SUV_{max}$) in the ROI was automatically calculated. The liver background $SUV_{max}$ was obtained from measurements in the areas of normal liver tissue beyond the lesion. According to the uptake extent of the hepatic metastases on PET cross-sectional imaging, lesions were divided into the following three types: type A was defined as lesion $^{18}$F-fluorodeoxyglucose ($^{18}$F-FDG) uptake significantly higher than liver background and could be detected clearly in the corresponding area of MIP imaging; type B was defined as lesion $^{18}$F-FDG uptake slightly higher than liver background and no significant hypermetabolism or only mild hypermetabolism could be detected on MIP imaging; and type C was defined as lesion's $^{18}$F-FDG uptake lower than, or comparable to the level of liver background radiotracer activity with no hypermetabolism detected on MIP imaging.

MR images were reviewed by two experienced radiologists using the double-blinded method. The location, morphology, size, margin, signal intensity (T1-weighted, T2-weighted, and diffusion-weighted images were defined as hypo-, iso-, or hyper-intense relative to liver parenchyma), and enhancement pattern (defined as lower than, equal to, or higher than liver parenchyma) of the GIST metastases were obtained using a picture archiving and communication system (PACS, Shida Co., Ltd., China) workstation.

### *Statistical analysis*

Statistical analyses were conducted using SPSS software (version, 22.0; IBM, Armonk, NY, USA). Continuous variables were described by means ± standard deviations or median (interquartile range), while categorical variables were described by frequencies and percentages. The Spearman's rank test was used to evaluate the correlation between the: (I) diameter and $SUV_{max}$ of liver metastases; and (II) the primary GIST tumor $SUV_{max}$ and the synchronous liver metastases $SUV_{max}$. A P value <0.05 was considered statistically significant.

## Results

A total of 90 GIST patients were found to have liver metastases. Of those, 32 patients received targeted therapy within 6 months of liver metastasis detection, 2 patients had synchronous malignancies (1 had nasopharyngeal carcinoma and another had cervical carcinoma), and 1 patient had diffuse liver metastases resulting in partial lesions could not be evaluated. Finally, 55 patients, including 21 females and 34 males with a mean age of 54.80±10.66 years (range, 28–78 years), were included in this retrospective study. Of these 55 patients, 4 GIST patients (2 stomach, 1 intestine, and 1 colon; 3 preoperative and 1 postoperative) underwent both PET/CT and MR scans at intervals of 1–6 days, 29 patients (4 stomach, 15 intestine, 5 duodenum, 1 esophagus, and 4 unknown; 16 preoperative and 13 postoperative) underwent PET/CT, and the remaining 22 patients (9 stomach, 8 intestine, 2 duodenum, 1 rectum, and 2 unknown; 11 preoperative and 11 postoperative) underwent MRI. All 55 GIST cases were pathologically confirmed by either surgery or biopsy. According to the United States National Institutes of Health GIST risk classification criteria [2008], 15 cases were diagnosed as high-risk (n=13), intermediate-risk (n=1), and low-risk (n=1) respectively, and the remaining 40 cases were not categorized because the mitotic index was not evaluated, owing to the small sample size from the biopsy. PET/CT imaging on 33 patients revealed that 11 had solitary metastases and 22 had multiple GIST liver metastases. MRI imaging of 26 patients revealed that 4 had solitary and 22 had multiple liver metastases. For the lesion-based analysis, the number of liver metastases detected by PET/CT and MR imaging was 113 and 109, respectively. A total of 23 lesions were pathologically confirmed and the remaining lesions were confirmed by imaging follow-up.

### *PET/CT imaging analysis*

The 113 GIST liver metastases were 0.6–14.6 cm [2.2 (1.5, 3. 9) cm] in diameter with a $SUV_{max}$ of 1.4–21.5 [3.6 (2.3, 5. 9)]. Of these lesions, 92.0% (104/113) had well-defined borders and 8.0% (9/113) had poorly defined or indistinct borders; 73.5% (83/113) had a homogeneous density (2 with homogeneous cystic change and 81 with soft tissue density), 26.5% (30/113) had a heterogeneous density (with necrosis or cystic degeneration or hemorrhage); and cystic degeneration or necrosis could be seen in a central or scattered distribution. The results of the PET visual analysis in $^{18}$F-FDG PET/CT of GIST liver metastases are shown in *Table 1*, and featured images of A, B, and C type lesions are shown in *Figure 1*. There was a weak correlation

 

**Table 1** Results of PET visual analysis in $^{18}$F-fluoro-2-deoxyglucose positron emission tomography/computed tomography of liver metastases in gastrointestinal stromal tumors

| Feature | Visual analysis types | Patients | Lesions | Diameter (cm) | $SUV_{max}$ | Liver background $SUV_{max}$ |
|---|---|---|---|---|---|---|
| All lesions | A | | 44 | 0.9–9.6 | 3.5–21.5 | 1.8–3.1 |
| | B | | 27 | 0.9–14.6 | 2.0–5.8 | 1.8–4.5 |
| | C | | 42 | 0.6–8.1 | 1.6–5.0 | 1.6–3.9 |
| Solitary metastases | A | 3 | 3 | 1.7–7.5 | 9.6–18.2 | 2.1–3.0 |
| | B | 4 | 4 | 1.3–2.4 | 3.0–5.2 | 2.1–4.5 |
| | C | 4 | 4 | 1.3–6.8 | 1.4–3.5 | 1.6–3.9 |
| Multiple metastases | A | 2 | 10 | 0.9–5.2 | 5.3–21.5 | 2.5–3.1 |
| | C | 5 | 16 | 0.6–8.1 | 1.6–3.3 | 1.9–3.5 |
| | AB | 4 | 15 | 0.9–9.6 | 2.0–13.4 | 1.5–2.9 |
| | AC | 2 | 7 | 1.6–6.0 | 1.9–17.3 | 2.0–2.3 |
| | BC | 2 | 7 | 1.1–8.0 | 2.2–5.8 | 2.5–3.7 |
| | ABC | 7 | 47 | 1.0–14.6 | 1.7–16.1 | 1.8–3.1 |

AB/AC/BC/ABC indicates the simultaneous presence of two or three types of the corresponding PET visual analysis in the same case with multiple liver metastases; PET, positron emission tomography; $SUV_{max}$, maximal standard uptake.

between the diameter of all GIST liver metastases and the $SUV_{max}$ ($r_s$=0.370, P<0.001). The $SUV_{max}$ of 66 synchronous liver metastases from 19 GIST cases were moderately correlated with the $SUV_{max}$ of the primary tumor ($r_s$=0.492, P<0.001).

### *MR imaging analysis*

The 109 liver metastases were 0.4–11.0 [2.1 (1.3, 3.3)] cm in diameter with well-defined borders in 100% (109/109) of the lesions. Compared with background liver parenchyma, all lesions showed hypointensity on T1-weighted images, hyperintensity on T2-weighted images, and hyperintensity on diffusion-weighted images. Cystic changes or necrosis (appearing as lower signals on T1-weighted images, higher signals on T2-weighted images, and hypointense areas on diffusion-weighted images) were observed in 35.8% (39/109) of the lesions, and 20.2% (22/109) of lesions had hemorrhage (appearing as patchy hyperintense areas on T1-weighted images and hyper- or hypo-intensity on T2-weighted images). On MR dynamic contrast-enhanced imaging, 90.8% (99/109) of GIST liver metastases showed heterogeneous enhancement in the arterial phase with diverse presentation, and 74.3% (81/109) of lesions had different enhancement patterns between margins and intratumoral parenchyma (*Figures 1*,*2*). The conventional MR dynamic enhancement features of GIST liver metastases are summarized in *Tables 2*,*3*. Of the 6 patients who underwent hepatobiliary phase scans, 3 patients showed liver metastases with ring-like hypo-enhancement margin and comparable intratumoral enhancement relative to liver.

A total of 14 liver metastases were detected in the 4 GIST patients who underwent both PET/CT and MR scans. There were 3 lesions from 2 patients which were missed on PET/CT imaging, but could be detected on MR imaging, with all 3 lesions showing no significantly increased radiotracer uptake as compared to background liver parenchyma. One lesion was 0.7 cm in diameter, and the other 2 lesions from one patient were 1.0 and 1.3 cm in diameter. These lesions could not be detected on unenhanced CT because of underlying fatty liver disease (*Figure 1*). By comparing metabolism with blood supply in the same metastases, we found that 6 lesions showed metabolic mismatch with blood supply, 5 lesions showed hyper-enhancement on MRI but with only mild or no metabolic increased radiotracer uptake on PET scan, and 1 lesion showed no significantly increased enhancement on MRI but increased radiotracer activity on PET scan.

## Discussion

The results of the present study demonstrated that GIST

 

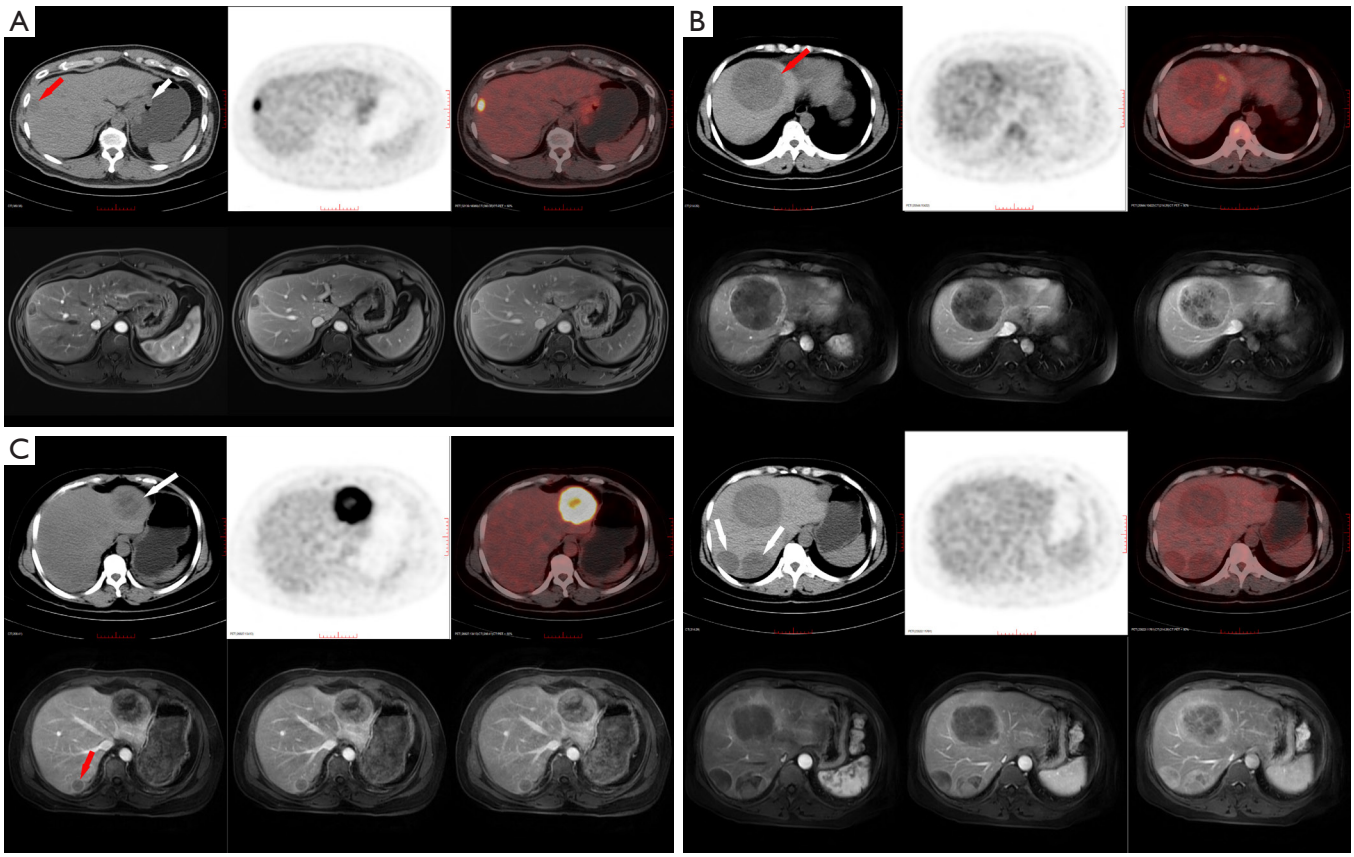


**Figure 1** Imaging findings of 3 GIST patients with liver metastases without treatment who underwent both $^{18}$F-FDG-PET/CT and MRI. (A) Imaging data of a 45-year-old man with solitary liver metastasis from gastric stromal tumor. CT image shows a hypodense nodule (red arrow) in the right lobe of the liver with unclear margins. PET image shows that the metabolism was significantly higher than the liver parenchyma, even higher than the primary tumor (white arrow), which was considered to be a type A lesion on visual analysis (hypermetabolism). Ring-like hyper-enhancement can be seen in the arterial and portal venous, and delayed phases and the intratumoral parenchyma showed gradual mild to moderate enhancement on MRI. (B) Imaging data of a 50-year-old female patient with multiple liver metastases from small intestinal stromal tumor. CT image shows multiple round masses in the liver with clear margins and slightly heterogeneous density. PET image of the largest lesion (red arrow) shows slightly higher metabolism in some areas of the mass, which was slightly higher than the liver parenchyma. Visual analysis showed a type B lesion (slightly hypermetabolism). The MR image showed rim enhancement and inner heterogeneous gradual enhancement, even partial areas was equal to or slightly higher than liver parenchymal in delayed phase. The other two lesions (white arrows) showed no hypermetabolism compared to the liver background, and no radioactive defect. These were type C lesions on visual analysis (iso- or hypo-metabolism). MRI shows marginal enhancement with inner heterogeneous gradual enhancement which was higher than liver parenchyma in the delayed phase. (C) Imaging data of a 53-year-old female patient with multiple liver metastases from colonic stromal tumor. The lesion in the left lobe of the liver (white arrow) showed significantly hypermetabolism on PET (type A lesion) with gradual enhancement on MRI. Another lesion in the right lobe (red arrow) was a missed diagnosis on PET/CT because of the presence of fatty liver disease, which showed no definite abnormal density on unenhanced CT and no hypermetabolism on PET. Ring-like enhancement of the margin and mild enhancement of the intratumoral parenchyma can be seen on MRI. GIST, gastrointestinal stromal tumor; $^{18}$F-FDG, $^{18}$F-fluorodeoxyglucose; PET, positron emission tomography; CT, computed tomography; MRI, magnetic resonance imaging.

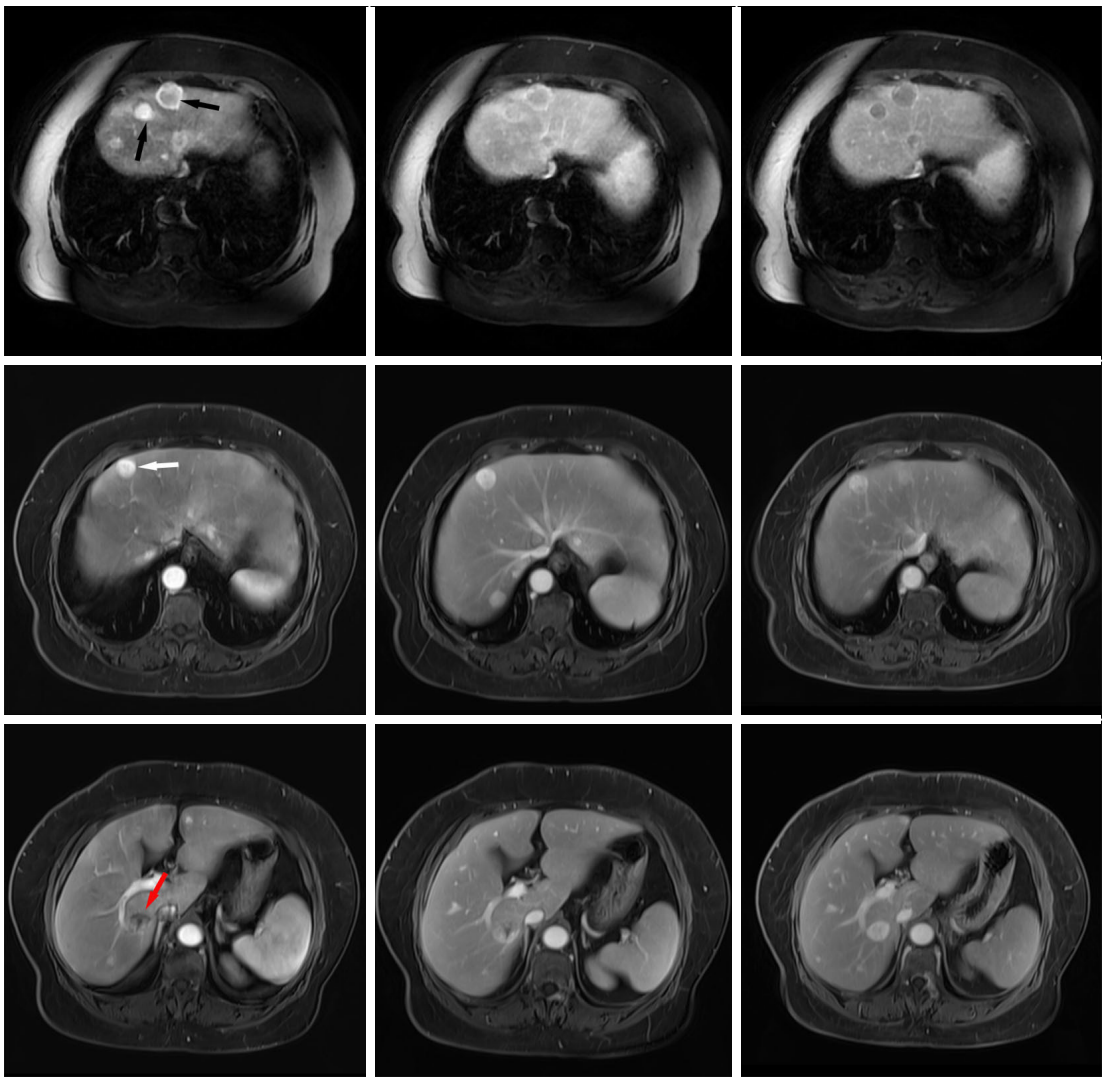

**Figure 2** Magnetic resonance imaging of a 68-year-old female patient with postoperative haptic recurrence 4 years after primary tumor resection shows different enhancement patterns. From left to right: arterial phase, portal venous phase, and delayed phase imaging at the same cross-sectional level. The first row of lesions (black arrows) shows obvious enhancement in the arterial phase, and decreased enhancement in the portal venous phase and delayed phase with marginal ring-like enhancement. The second row of lesions (white arrow) show obvious enhancement in all three phases. The third row of lesions (red arrow) show heterogeneous gradual enhancement in the arterial and portal venous phases, and obvious enhancement in the delayed phase.

liver metastases differ considerably in terms of $^{18}$F-FDG PET/CT metabolic rate/radiotracer activity. The imaging features of GIST liver metastases on $^{18}$F-FDG PET/CT can be summarized as follows: (I) There are usually multiple GIST liver metastases which may involve both lobes. On low-dose unenhanced CT, they often appear as rounded shapes with a well-defined border and either homogeneous or heterogeneous density. These lesions may be accompanied by cystic changes, necrosis, or hemorrhage, which can be centrally located or scattered. In contrast, adenocarcinoma liver metastases tend to show low density cystic or necrotic changes that are more often centrally located, meanwhile, hemorrhage is relatively rare. (II) PET imaging shows a variety of findings, and multiple liver metastatic lesions in the same case can show a consistent appearance, as well as the presence of lesions that are metabolically lower, equal, or higher than background liver parenchyma. (III) For lesions with a

 

**Table 2** The enhancement degree of gastrointestinal stromal tumors liver metastases relative to normal liver in conventional magnetic resonance contrast-enhancement imaging

| Enhancement degree | Arterial phase | Portal venous phase | Delayed phase |
|---|---|---|---|
| Margin | | | |
| Ring-like hyper-enhancement | 62 | 70 | 62 |
| Ring-like hypo-enhancement | 2 | 1 | 14 |
| Intratumoral parenchyma | | | |
| Hyper-intense | 31 | 19 | 27 |
| Iso-intense | 3 | 14 | 22 |
| Hypo-intense | 75 | 76 | 60 |
| Ill-defined[†] | 3 | 14 | 15 |

[†], both lesion margins and parenchyma appeared ill defined.

**Table 3** The enhancement pattern of gastrointestinal stromal tumors liver metastases relative to normal liver in conventional magnetic resonance contrast-enhancement imaging

| Enhancement pattern | No. of metastases (n=109) | Diameter (cm) |
|---|---|---|
| Margin | | |
| Ring-like hyper-enhancement, persistent | 43 | 0.6–9.3 |
| Ring-like hyper-enhancement in arterial phase, disappeared posteriorly | 5 | 1.1–8.5 |
| Ring-like hyper-enhancement changes to hypo-enhancement | 14 | 0.8–2.4 |
| Without of ring-like hyper-enhancement in arterial phase, appeared posteriorly | 17 | 1.5–11.0 |
| Ring-like hypo-enhancement changes to hyper-enhancement | 2 | 2.4–6.0 |
| Always without ring-like enhancement or similar to Intratumoral parenchyma | 28 | 0.4–4.5 |
| Intratumoral parenchyma | | |
| Homogeneous arterial phase, persistent | 25 | 0.6–6.0 |
| Homogeneous arterial phase, reduced | 6 | 0.6–2.7 |
| Gradual enhancement | 78 | 0.4–11.0 |

higher metabolic rate on PET imaging, those with larger volumes mostly showed heterogeneous metabolism, especially slightly hypermetabolic lesions that often showed scattered heterogenous and slight hypermetabolic shadows distributed on the lesion area. Metabolic defects were less frequently observed when the difference between lesion's metabolism and liver background was not obvious, which might be explained by the fact that the lesions were cystic in nature but still had less solid tumor components distributed diffusely. (IV) Though cystic metastasis is rare and has only been documented in case reports (24,25), misdiagnosis as a cyst should be avoided when the lesion is small, with a well-defined margin and without increased radiotracer activity on PET scan.

There was only a poor correlation between the $SUV_{max}$ of GIST liver metastases and lesion diameter in our study. In addition, 37.2% (42/113) of GIST liver metastases in our analysis showed hypometabolism, and the largest one was up to 8.1 cm in diameter. Typically, except for lesions less than 1.0 cm in diameter, most liver metastases from malignant tumors such as colon cancer, lung cancer, and breast cancer show hypermetabolism, suggesting that there is certain level of metabolic rate specificity of GIST liver metastases. However, owing to limited sample size, the lack of available pathological data from liver metastatic lesions, and the limited number of related publications in

 

the literature, the reasons could not be further analyzed in the current investigation. A report by Min (26) suggested that GISTs have considerable variation in the general appearance of cells and cytoplasmic organelles, as well as the relationship between tumor cells, stroma and intercellular stromal contents depending on their original site of the gastrointestinal tract. Parts of GIST liver metastases in our study showed mild or no hypermetabolism on $^{18}$F-FDG PET/CT, which may be related to more empty cytoplasmic vacuoles. In addition, we speculated that the differences in $^{18}$F-FDG PET/CT features of liver metastases might be related to histopathologic, immunohistochemical, and genetic characteristics of the tumor, necrosis, and hemorrhage. Although only 4 patients underwent both MRI and PET/CT, we found that the lesions were prone to missed diagnosis on PET/CT when they were hypometabolic and small in size or in setting of background fatty liver disease. It is known that GIST liver metastases can be cystic, necrotic, and even increase in size after treatment with targeted therapies (27,28). For liver metastases with low or slightly higher metabolism before treatment, PET/CT imaging may yield false-negative results and cannot truly reflect the degree of tumor viability during follow-up scans, and MRI may be more accurate in estimating treatment efficacy by evaluating the presence of hyper-enhancing components.

MRI performed using various sequences is more accurate than CT in characterizing different tumor components. Therefore, this study selected GIST patients with liver metastases who underwent MRI examination for inclusion. Except for tumor morphology, margins, cystic or necrotic changes, hemorrhage, and other similar features described above on PET/CT, the most characteristic imaging feature of GIST liver metastases on MRI are diverse in presentation on dynamic contrast-enhanced scans. First, rim enhancement pattern of most lesions does not correlate with pattern of its intra-tumoral parenchyma enhancement, which suggests that GIST liver metastasis has a dual blood supply. According to the distinct interface between metastasis and the adjacent normal liver parenchyma, liver metastases present three different histopathological growth patterns (HGPs), including desmoplastic, replacement, and pushing HGPs, and this may impact overall survival after surgery for colorectal liver metastases (29). Li *et al.* (30) retrospectively analyzed MRI features of HGPs of colorectal liver metastases and demonstrated that MRI could help differentiate replacement HGPs and non-replacement HGPs. In our study, although not pathologically confirmed, combined with the morphology, margins of GIST liver metastases, and ring-like hyper-enhancement on dynamic contrast-enhanced scans, we speculated that the pathophysiological growth pattern of GIST liver metastases might be dominated by pushing HGP. In the pushing HGP, the metastasis pushes away and compresses the adjacent hepatocellular plates, without invading the hepatocellular plates, and blood supply is obtained by sprouting neovascularization (29). GIST liver metastases grow expansively, thus pushing out the surrounding liver parenchyma and form a clear margin. This may cause perfusion abnormalities in the surrounding liver parenchyma, leading to a blood perfusion differential between the margin and intratumoral parenchyma of the lesion. Second, ring-like hyper-enhancement can be seen in most GIST liver metastases, even at diameters less than 1.0 cm. The rim enhancement of the lesion can appear in various ways such as continuous hyper-enhancement or appear, disappear, or transform into ring-like hypo-enhancement during delayed scan images. Third, the intratumoral parenchyma of some GIST metastasis can show marked enhancement in the arterial phase, with the majority of lesions showing heterogeneous progressive enhancement, which may be similar to or higher than the liver parenchyma at delayed phase or later time points. Due to variability of MRI findings in GIST liver metastases, small lesions may be misdiagnosed as hemangioma, hepatic adenoma, focal nodular hyperplasia, and so on due to marked hyperenhancement, and this is especially challenging for solitary metastases. They may also be misdiagnosed as a cyst when it contains more cystic components and shows lower-signal intensity on T1-weighted images, higher-signal intensity on T2-weighted images, and lack of visible enhancement. Therefore, a through differential diagnosis should be emphasized for intrahepatic lesions detected in newly diagnosed or follow-up examinations, despite presence of atypical imaging findings. The clinical management decisions should be taken after multidisciplinary tumor board discussions.

For most lesions, it is not difficult to diagnose liver metastasis by combining the history of GIST with MRI or $^{18}$F-FDG PET/CT imaging findings. However, misdiagnosis and/or missed diagnosis situations are still difficult to avoid for some small, solitary, or poorly defined lesions. Summarizing the imaging characteristics of GIST may help in the diagnosis of some of these challenging lesions. In addition, the diverse imaging findings of GIST liver metastases confirmed by our study may be instructive

 

in the selection of best imaging modalities to be used after targeted therapy to avoid false negatives. Because of the diverse presentation of GIST liver metastases on MRI and PET/CT, for some liver lesions with qualitative difficulties, the combination of both imaging methods can evaluate the lesions' metabolism and blood perfusion simultaneously, which may be helpful for diagnosis. PET/MR has become more widely used in recent years and has been proven to be a quite efficient diagnostic modality compared to PET/CT, MR, and CT for the diagnosis of liver metastases (31,32), although these literatures selected liver metastases from other common tumors and it may be equally applicable to GIST liver metastases. There were some limitations in our study. First, only a small sample size was analyzed, especially patients who underwent both $^{18}$F-FDG PET/CT and MRI. Furthermore, only metabolic rate/radiotracer activity and blood perfusion characteristics of GIST liver metastases were described, without further analysis of their correlation and diagnostic efficacy. Due to the limited postoperative pathological data of GIST liver metastases, it was impossible to analyze the reasons behind these diverse imaging findings. Further studies with a larger sample size are required to examine exact nature of any existing radio-pathological correlations.

In summary, GIST liver metastasis usually has well-defined margins and can be associated with cystic change, necrosis, or hemorrhage, which can appear diversely on both $^{18}$F-FDG PET/CT and MR imaging. Lesions can appear significantly hypermetabolic, slightly hypermetabolic, or hypometabolic on PET, and the degree of metabolism/radiotracer activity correlates poorly with the size of the lesion. Radiotracer activity defect is rare on PET imaging of hepatic lesions. On MR imaging, GIST liver metastases demonstrate a dual blood supply pattern, with ring-like enhancement observed in most lesions. The intratumoral parenchyma of metastasis shows marked enhancement or heterogeneous progressive enhancement. However, smaller GIST liver metastasis may demonstrate hypometabolism on PET, or marked enhancement on MRI, making this subset more difficult to diagnose. Therefore, tissue sampling or close follow-up is warranted to avoid misdiagnosis.

## Acknowledgments

The authors appreciate the academic support from the AME Gastrointestinal Stromal Tumor Collaborative Group.
*Funding:* None.

## Footnote

*Reporting Checklist:* The authors have completed the STROBE reporting checklist. Available at https://atm.amegroups.com/article/view/10.21037/atm-22-5181/rc

*Data Sharing Statement:* Available at https://atm.amegroups.com/article/view/10.21037/atm-22-5181/dss

*Conflicts of Interest:* All authors have completed the ICMJE uniform disclosure form (available at https://atm.amegroups.com/article/view/10.21037/atm-22-5181/coif). DR received consulting fees from Medtronic's liver ablation division from speaker's bureau and medical device development unit. The other authors have no conflicts of interest to declare.

*Ethical Statement:* The authors are accountable for all aspects of the work in ensuring that questions related to the accuracy or integrity of any part of the work are appropriately investigated and resolved. The study was conducted in accordance with the Declaration of Helsinki (as revised in 2013). The study was approved by the Medical Ethics board of Fujian Cancer Hospital (No. K2022-131-01) and informed consent was taken from all individual participants.



## References

1. Levy AD, Remotti HE, Thompson WM, et al. Gastrointestinal stromal tumours: radiologic feature with pathologic correlation. Radiographics 2003;23:283-304.
2. Arshad J, Costa PA, Barreto-Coelho P, et al. Immunotherapy Strategies for Gastrointestinal Stromal Tumor. Cancers (Basel) 2021;13:3525.
3. Gharibo M, Patrick-Miller L, Zheng L, et al. A phase II trial of imatinib mesylate in patients with metastatic pancreatic cancer. Pancreas 2008;36:341-5.

 

4. Ambrosio MR, Rocca BJ, Mastrogiulio MG, et al. Cystic gastrointestinal stromal tumors of the pancreas simulating cystoadenocarcinoma. Report of three cases and short review of the literature. Histol Histopathol 2014;29:1583-91.
5. Tateishi U, Hasegawa T, Satake M, et al. Gastrointestinal stromal tumor. Correlation of computed tomography findings with tumor grade and mortality. J Comput Assist Tomogr 2003;27:792-8.
6. DeMatteo RP, Lewis JJ, Leung D, et al. Two hundred gastrointestinal stromal tumors: recurrence patterns and prognostic factors for survival. Ann Surg 2000;231:51-8.
7. Shima Y, Horimi T, Ishikawa T, et al. Aggressive surgery for liver metastases from gastrointestinal stromal tumors. J Hepatobiliary Pancreat Surg 2003;10:77-80.
8. Gomez D, Al-Mukthar A, Menon KV, et al. Aggressive surgical resection for the management of hepatic metastases from gastrointestinal stromal tumours: a single centre experience. HPB (Oxford) 2007;9:64-70.
9. Ginori A, Scaramuzzino F, Marsili S, et al. Late hepatic metastasis from a duodenal gastrointestinal stromal tumor (29 years after surgery): report of a case and review of the literature. Int J Surg Pathol 2015;23:317-21.
10. Ishizaki M, Uno F, Yoshida R, et al. Very delayed liver metastasis from small bowel gastrointestinal stromal tumor (32 years after resection of the small bowel GIST): Report of a case. Int J Surg Case Rep 2020;76:156-60.
11. Takano Y, Yamawaki M, Noda J, et al. A Case of Liver Metastasis from Small Intestinal Gastrointestinal Stromal Tumor 25 Years after Surgery including Autopsy Findings. Case Rep Gastrointest Med 2021;2021:6642427.
12. Yang DY, Wang X, Yuan WJ, et al. Metastatic pattern and prognosis of gastrointestinal stromal tumor (GIST): a SEER-based analysis. Clin Transl Oncol 2019;21:1654-62.
13. Altini C, Lavelli V, Ruta R, et al. Typical and atypical PET/CT findings in non-cancerous conditions. Hell J Nucl Med 2020;23:48-59.
14. Kalkmann J, Zeile M, Antoch G, et al. Consensus report on the radiological management of patients with gastrointestinal stromal tumours (GIST): recommendations of the German GIST Imaging Working Group. Cancer Imaging 2012;12:126-35.
15. Zheng T, Du J, Yang L, et al. Evaluation of risk classifications for gastrointestinal stromal tumor using multi-parameter Magnetic Resonance analysis. Abdom Radiol (NY) 2021;46:1506-18.
16. Kim SJ, Lee SW. Performance of F-18 FDG PET/CT for predicting malignant potential of gastrointestinal stromal tumors: A systematic review and meta-analysis. J Gastroenterol Hepatol 2018;33:576-82.
17. Li S, Lin D, Tang M, et al. Value of 18F-FDG PET/CT for differentiating diagnosis between malignant and benign primary gastric gastrointestinal mesenchymal tumors: a single-center retrospective study. J Gastrointest Oncol 2022;13:637-46.
18. Yokoyama K, Tsuchiya J, Nakamoto Y, et al. Additional Value of 18FFDG PET or PET/CT for Response Assessment of Patients with Gastrointestinal Stromal Tumor Undergoing Molecular Targeted Therapy: A Meta-Analysis. Diagnostics (Basel) 2021;11:475.
19. Gong NJ, Wong CS, Chu YC, et al. Treatment response monitoring in patients with gastrointestinal stromal tumor using diffusion-weighted imaging: preliminary results in comparison with positron emission tomography/computed tomography. NMR Biomed 2013;26:185-92.
20. Albano D, Mattia B, Giubbini R, et al. Role of 18F-FDG PET/CT in restaging and follow-up of patients with GIST. Abdom Radiol (NY) 2020;45:644-51.
21. Xue A, Gao X, He Y, et al. Role of Surgery in the Management of Liver Metastases From Gastrointestinal Stromal Tumors. Front Oncol 2022;12:903487.
22. Sutton TL, Walker BS, Billingsley KG, et al. Hepatic metastases in gastrointestinal stromal tumors: oncologic outcomes with curative-intent hepatectomy, resection of treatment-resistant disease, and tyrosine kinase inhibitor therapy alone. HPB (Oxford) 2022;24:986-93.
23. Zhu J, Yang Y, Zhou L, et al. A long-term follow-up of the imatinib mesylate treatment for the patients with recurrent gastrointestinal stromal tumor (GIST): the liver metastasis and the outcome. BMC Cancer 2010;10:199.
24. Zonios D, Soula M, Archimandritis AJ, et al. Cystlike hepatic metastases from gastrointestinal stromal tumors could be seen before any treatment. AJR Am J Roentgenol 2003;181:282; author reply 282.
25. Sakata M, Kaneyoshi T, Fushimi T, et al. Rare cause of cystic liver lesions: Liver metastasis of gastrointestinal stromal tumors. JGH Open 2021;5:408-9.
26. Min KW. Gastrointestinal stromal tumor: an ultrastructural investigation on regional differences with considerations on their histogenesis. Ultrastruct Pathol 2010;34:174-88.
27. Chen MY, Bechtold RE, Savage PD. Cystic changes in hepatic metastases from gastrointestinal stromal tumors (GISTs) treated with Gleevec (imatinib mesylate). AJR Am J Roentgenol 2002;179:1059-62.
28. Boonsirikamchai P, Podoloff DA, Choi H. Imaging of

 

gastrointestinal stromal tumors and assessment of benefit from systemic therapy. Hematol Oncol Clin North Am 2009;23:35-48, vii.
29. van Dam PJ, van der Stok EP, Teuwen LA, et al. International consensus guidelines for scoring the histopathological growth patterns of liver metastasis. Br J Cancer 2017;117:1427-41.
30. Li WH, Wang S, Liu Y, et al. Differentiation of histopathological growth patterns of colorectal liver metastases by MRI features. Quant Imaging Med Surg 2022;12:608-17.
31. Zhou N, Meng X, Zhang Y, et al. Diagnostic Value of Delayed PET/MR in Liver Metastasis in Comparison With PET/CT. Front Oncol 2021;11:717687.
32. Yong TW, Yuan ZZ, Jun Z, et al. Sensitivity of PET/MR images in liver metastases from colorectal carcinoma. Hell J Nucl Med 2011;14:264-8.

(English Language Editor: J. Teoh)

**Cite this article as:** Lyu Q, Lin D, Tang M, Liu D, Zhang J, Wang Y, Shelat VG, Raissi D, Ostwal V, Chen X, Li S. $^{18}$F-FDG PET/CT and MR imaging features of liver metastases in gastrointestinal stromal tumors: a cross-sectional analysis. Ann Transl Med 2022;10(22):1220. doi: 10.21037/atm-22-5181

 